CHIN. PHYS. LETT. Vol. 30, No. 4 (2013) 043102

First Principles Study of Single Wall TiO_2 Nanotubes Rolled by Anatase Monolayers

ZHANG Hai-Yang(张海洋)**, DONG Shun-Le(董顺乐)

Department of Physics, Ocean University of China, Qingdao 266100

(Received 20 December 2012)

Titanium dioxide (TiO_2) nanotubes have been widely investigated for their potential applications in solar cells, hydrogen production, and catalysis. We study three types of TiO_2 nanotubes constructed from anatase TiO_2 monolayers with density functional-based tight binding methods employing the DFTB+ code. The dependences of the strain energies, structural and electronic properties on the radii of the tubes are investigated in the 3–10 Å range. In addition, the present calculations indicate that the electronic band gap of all types of TiO_2 nanotubes is proportional to their diameters. Chiral (n, m) tubes have smaller band gaps than $(n, 0)$ and $(m, 0)$ tubes, which can be prepared for absorbing the visible spectrum of solar energy.

PACS: 31.15.es 31.15.aq 03.65.−w DOI: 10.1088/0256-307X/30/4/043102

Titanium dioxide (TiO_2) nanotubes have attracted much attention because of their unique chemical properties, including high photocatalytic activity, strong oxidizing power, non-toxicity, large surface area, high surface-to-volume ratio and unique optical property. TiO_2 nanotubes were widely investigated for their potential applications[1,2] such as photocatalysis, dyed-sensitive solar cells (DSSC), gas sensors, air and water purifiers, and so on. Various methods for the syntheses of the TiO_2 nanotubes were proposed, causing a large variety of morphology and probably the properties of the TiO_2 nanotubes. For example, the diameters and structure of the walls of nanotubes may be very different, mainly depending on the varying preparation methods.[5,6] Hitherto, in general, there are three geometry configurations of the tube walls, which are widely adopted, including trititanate,[5] lepidocrocite-like[4] and an anatase structure.[3] The anatase structure was firstly found in nanotubes prepared by the hydrothermal method from anatase powder based on XAED and HRTEM investigations several years ago.[7] The lepidocrocite-like structure is supported by the electron diffraction study by Akita,[8] who proposed a crystalline structure of nanotubes different from that of anatase. The trititanate structure $H_2Ti_3O_7$, also found by XRD and SAED investigations,[5] provided another proper model for TiO_2 nanotubes. In spite of numerous experimental results, the atomic-level information on the structure of TiO_2 nanotubes is still ambiguous.

As is well known, in TiO_2 anatase morphology, there are two low energy surfaces: (001) and (101), which are common for natural crystals. One-dimensional TiO_2-based nanotubes would be formed by rolling surfaces (001) and (101). An ultrathin anatase (001) surface cannot form a feasible titania tube-structure because of its distinct reconstructions. The two-layer (2-ML) thick anatase (001) film would rearrange spontaneously to a lepidocrocite-like structure and eventually form a lepidocrocite-like nanotube.[11,12] Enyashin and Seifert[13] studied the structural properties, the stability and the electronic properties of various nanostructures based on titania layer modifications (anatase and lepidocrocite) using the density-functional tight-binding method (DFTB). They found that the anatase nanotubes are the most stable nanostructure of TiO_2. Furthermore, their stability increases (the strain energy decreases) when their radii grow. Ferrari *et al.*[14] studied a series of anatase nanotubes of 3-ML (001) films, which are more stable than the corresponding surface. In addition, $(n, 0)$ and $(0, m)$ nanotubes were constructed by rolling an anatase (101) sheet along the [101] and [010] directions, respectively, by Bandura and Evarestov.[15] In their study, the systems were calculated by the first principles LCAO with a hybrid HF/KS(PBE0) exchange-correlation functional. They found that the energy band gap of the TiO_2 nanotubes increases from 4.7 eV to 5.4 eV when the tubes' radius changes from 3.61 Å to 9.92 Å and the strain energy is larger for $(n, 0)$ than that for $(0, m)$ nanotubes in a similar radius.

In this Letter, a systematical study is reported in detail, with the structural and electronic properties of some anatase nanotubes. The electronic data of the TiO_2 nanotubes is of great interest for their potential applications, such as in optoelectronic devices and photocatalysts. We propose and examine three models of TiO_2 nanotubes which are optimized by employing the density-functional tight-binding method (DFTB+). The structures of the three models are distinctly different and have unique electronic properties. In addition, the band gaps of the nanotubes decrease when their diameters increase.

The bulk TiO_2 crystal structure in the anatase phase is optimized by the DFTB+ code package[16] based density functional tight binding (DFTB) method. Three parameters corresponding to the

**Corresponding author. Email: zhy88881111@163.com; 41710240@qq.com

© 2013 Chinese Physical Society and IOP Publishing Ltd

structure are listed in Table 1. In general, the theoretical results agree well with the experiment. The band gap is up to 3.21 eV higher than the results by DFT and LCAO, but much more closed to the experimental data. The monolayer (or slab) structure is formed by cleaving the anatase bulk along the $[10\bar{1}]$ and [010] directions. This 2-D periodic facet could be spanned by the periodic unit vector $\boldsymbol{a}_1$ and $\boldsymbol{a}_2$ of the unrelaxed monolayer, where $a_1 = a$ and $a_2 = c$, as shown in Fig. 1.

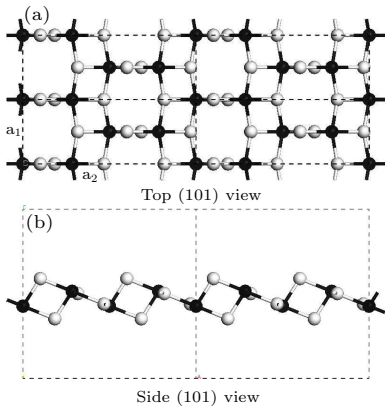


Fig. 1. The (2 × 2) anatase (101) monolayer structure shown in top (101) and side (010) views. The white and black balls represent the oxygen and titanium atoms, respectively. The unit vectors $\boldsymbol{a}_1$ and $\boldsymbol{a}_2$ represent the periodicity of the anatase (101) monolayer structure in the [010] and $[10\bar{1}]$ directions.

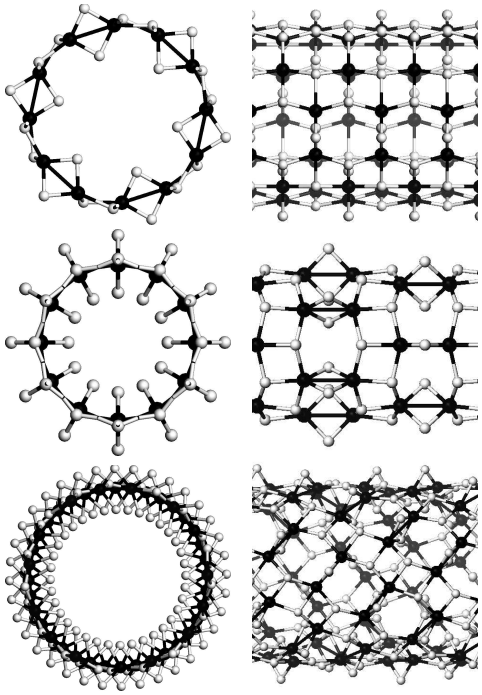


Fig. 2. The wall structure of the optimized $(0,3)$, $(6,0)$ and $(6,3)$ nanotubes at the top (left) and side (right) views. The white balls represent the oxygen atoms, while the black ones represent titanium atoms.

The one-dimensional (1-D) TiO_2 nanotubes were formed by rolling a 2-D lamellar structure, which was proposed by Wang *et al.*[7] Compared with the graphene, the topologic structure of the anatase monolayer shown in Fig. 1 displays obvious differences along the $\boldsymbol{a}_1$ and $\boldsymbol{a}_2$ directions. Thus, we have investigated the anatase nanotubes of three types: $(0,m)$, $(n,0)$ and chiral (n,m). According to the method of Wang *et al.*,[7] a TiO_2 nanotube model could be produced by wrapping the anatase (101) facet along the $\boldsymbol{a}_1$, $\boldsymbol{a}_2$ or chiral vector $\boldsymbol{t}$ direction where $\boldsymbol{t}$=$n\boldsymbol{a}_1 + m\boldsymbol{a}_2$, which is normal to the axis of the nanotubes. The chiral angle α was defined as $\alpha = \arctan(ma_2/na_1)$. In addition, we introduce the spiral differential angle $\Delta\theta = n(a_1)^2/(na_1)^2 + (ma_2)^2 \times 2\pi$ to describe the rotation of the definite nanotube unit which contains $12 \times m$ atoms. The degree of angle $\Delta\theta$ absolutely depends on m, n, a_1 and a_2. A specific spiral differential angle $\Delta\theta$ (Table 1) could be achieved by selecting the specific value of m and n and adjusting the lattice parameters a and c. The chiral TiO_2 nanotubes with definite periodic length ($L = 2\pi R \times \alpha$) are modestly reconstructed by choosing a reasonable value of parameter c.

All the TiO_2 nanotube calculations in this study are performed using the DFTB+ code package. A tetragonal supercell $30 \times 30 \times L$ Å^3 is employed with a length of L equaling the periodic length of the nanotubes along the Z direction. The distance between two contiguous tubes is set to be more than 10 Å to avoid interaction between them. The Brillouin zone of the model is sampled by $1 \times 1 \times 8$ K-points using the Monkhorst-pack scheme for $(0,m)$ and $(n,0)$ tubes, as well as $1 \times 1 \times 4$ K-points for the (n,m) cases. Convergence test calculations confirm that the size of the supercell and K-points could not affect the result.

Table 1. The parameters and band gap of the anatase lattice and (101) monolayer produced by DFTB+ and other calculation packages.

	a (Å)	c (Å)	d (Å)	Band gap (eV)
DFTB+	3.922	9.368	1.987	3.21
LCAO[15]	3.784	9.508	1.972	4.0
DFT[12]	3.803	9.603	2.000	2.08
Experimental data[18]	3.784	9.515	1.980	3.2
(101)monolayer DFTB+	3.406	10.192		3.44

Table 2. The structure parameters of the chiral nanotube (n,m).

(n,m)	$\Delta\theta$ (deg)	α (deg)	k	a (Å)	c (Å)	L (Å)	R (Å)
(3,2)	30	57.9721	12	3.9215	9.4034	40.75	3.7448
(4,2)	30	52.9132	12	3.9215	10.3753	38.42	4.3241
(6,3)	20	52.9132	18	3.9215	10.3753	57.63	6.4861
(8,3)	22.5	42.8312	16	3.9215	9.6942	44.37	7.0612

The indirect and direct energy band gaps E_g are given in Table 3 for the $(0,m)$ and $(n,0)$ tubes, respectively. However, these band gaps are closed to the bulk energy gap 3.2 eV and less than the monolayer band gap 4.44 eV. The strain energy E_s of the optimized tubes was calculated as $E_s = (E_{nt} - E_{layer})/N_{unit}$, where E_{nt} and E_{layer} are the energies of the optimized nanotube and monolayer, respectively; and N_{unit} is the number of the TiO_2 molecule in a nanotube. The

strain energy is well used to weight the stability of the nanotubes' structure due to different curvatures. It is clearly seen that the strain energies E_s of the $(0, m)$ and $(n, 0)$ tubes both increase continuously with their radii increasing, as listed in Table 3. Moreover, the $(0, m)$ tubes are more stable than the $(n, 0)$ ones in these cases. The structure of the tubes becomes more symmetrical and their radii become slightly less after optimization. The bond length between the bridging O and Ti atoms reduces to 1.85 Å, which is less than the O–Ti bond length of the relaxed bulk by 0.14 Å, reflecting the bigger charge overlap populations and lower polarity of the tubes than the bulk ones. The bridging oxygen atoms (the outermost oxygen atom of nanotubes in Fig. 2) are not saturated with high oxidation and hydrogen adsorption capacity. Compared to the bulk, the cylindrical structure of the tubes has a higher surface activity and catalytic because of their quite large exposed surface area.

Table 3. The properties of relaxed anatase $(n, 0)$ and $(m, 0)$ nanotubes. N is the total number of atoms.

Nanotubes structure	N	E_s (meV)	E_g	Radius R (Å)		Length L (Å)	
$(0, m)$			indirect	unrelaxed	relaxed	unrelaxed	relaxed
3	36	215.2	3.15	4.8489	4.8074	3.921	3.752
4	48	204.1	3.26	6.4651	6.4070	3.921	3.778
5	60	148.0	3.40	8.0814	8.0321	3.921	3.791
$(n, 0)$			Direct				
6	72	312.2	3.13	3.7448	3.6357	10.07	10.001
7	84	261.5	3.29	4.3689	4.2024	10.07	10.202
8	96	241.4	3.32	4.9930	4.7021	10.07	10.303

Table 4. The geometrical parameters and strain energies of the (n, m) nanotubes.

Nanotube structure (n, m)	N (atom numbers)	Radius R (Å)		E_s (meV)	E_g (eV)
		unrelaxed	relaxed		
(3,2)	288	3.7448	3.6627	410.9	2.95
(4,2)	288	4.1318	4.0276	372.3	3.06
(6,3)	648	6.4861	5.8063	299.6	3.18
(8,3)	576	7.0612	6.5934	267.5	3.28

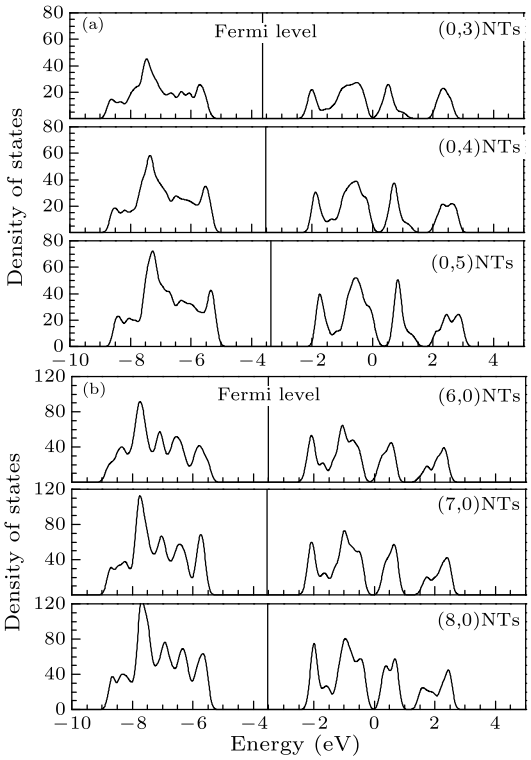


Fig. 3. The density of states curve of $(0, m)$ and $(n, 0)$ nanotubes (NTs).

The total density of state (TDOS) curves of the $(0, m)$ and $(n, 0)$ tubes near the Fermi level are shown in Fig. 3. The distributions of the density of states of the $(0, m)$ and $(n, 0)$ tubes almost remain unchanged when n and m are given with different values, respectively. On the contrary, the Fermi energy, the highest occupied molecular orbital (HOMO) and the lower unoccupied molecular orbital (LUMO) of the $(0, m)$ tubes increase with their radii increasing. However, the TDOS curves of the $(n, 0)$ tubes hardly change, and on their valence band the TDOS curves produce four obvious characteristic peaks to present strong locality of the density of the electronic states. These peaks are attributed to weak hybridization of the $2p$ orbital of the bridging oxygen atoms and the $2p$ orbital of the three fold-coordinated oxygen atoms (located in the middle of the tubes).

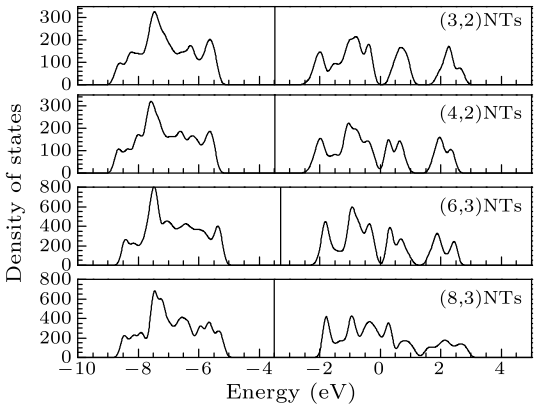


Fig. 4. The DOS pictures of several typical (m, n) nanotubes.

The (n,m) chiral tubes apparently have a larger radii than the $(0,m)$ and $(n,0)$ tubes, so their tension is smaller due to their smaller curvature. The geometries of some of the typical chiral TiO_2 nanotubes listed in Table 4 are optimized. It is seen that all the selected tubes' radii reduce during optimization, and their changes are obviously different: 0.04–0.06 Å for the $(0,m)$ cases, 0.1–0.29 Å for the $(n,0)$ cases, and 0.08–0.5 Å for the (n,m) cases. Such a change in their radii is directly proportional to radii R of the relative tubes. Moreover, after optimization, the strain energy of the (n,m) tubes is more than the other tubes partly owing to the reconstruction. However, like the $(0,m)$ and $(n,0)$ ones, the strain energy of the chiral (n,m) tubes decrease with increasing radius R, as shown in Fig. 6. In addition, the three types of tubes can be served as stable morphology and structure because of the small strain energy mostly under 0.4 eV. The energy gaps E_g are also collected in Tables 3 and 4 for the relaxed atomic structures of all the nanotubes. Their band gaps increase slightly as their radii increases, in agreement with the results of the previous calculations,[19–22] and move to the energy gap 3.44 eV of the unrolled optimized slab. The band gap of the (n,m) tubes is markedly less than the $(n,0)$ and $(0,m)$ tubes when the same radii are considered.

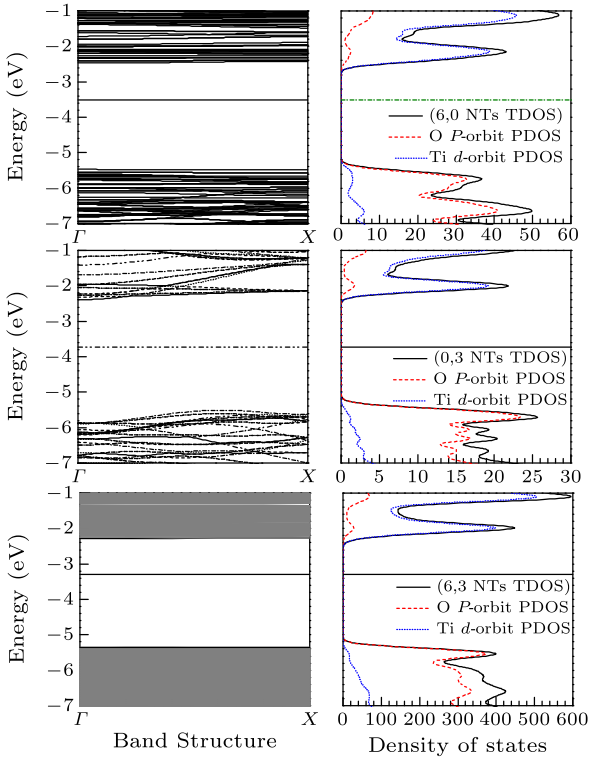


Fig. 5. The structure of the bands and the projected density of states (TDOS/PDOS) of the (6,0), (0,3) and (6,3) nanotubes.

However, in contradiction with the findings of Ref. [15], not all TiO_2 nanotube band gaps are larger than the bulk anatase band gaps ($E_g = 3.21$ eV). This contradiction can be explained by the different approaches to the structure optimization, because the authors of Ref. [15] used the PBE0 Hamiltonian in the structure optimization and the electronic structure calculations.

All the TiO_2 nanotubes listed here are semiconductors with wide-band gaps from 2.95 eV to 3.4 eV. In order to gain deeper insights into the fact that the chirality and curvature of the tube can affect the electron structures of TiO_2 nanotubes, we compute the energy band structures, and the total and projected density of states of the selected cases, as illustrated in Fig. 5. The densities of the states near the Fermi level for the $(0,3)$, $(6,0)$ and $(6,3)$ nanotubes are different, due to different chirality and reconstruction of the nanotube walls. In the three cases, the lower conduction bands are predominantly contributed to by the Ti $3d$ states, and the upper valence bands come from the $2p$ states of the O atoms. The DOS in the valence band region of Ti and O shows the maximum density in the same energy region, indicating a large covalent contribution to the Ti–O bond. In addition, there is a trend as shown in Fig. 6 that the widening of the energy gaps and the elimination of the strain of all the nanotubes with the increase in the diameter of the tubes can be traced to the decrease in the Ti–O bond lengths perpendicular to the tubes' axis.

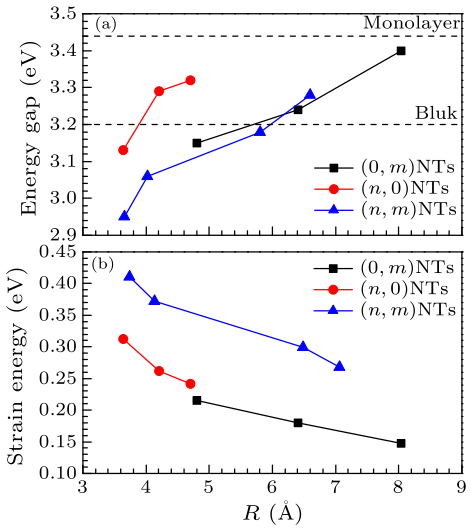


Fig. 6. The energy gaps and strain energies of the nanotubes.

Each of the three types of TiO_2 nanotubes, ($(0,m)$, $(n,0)$ and (n,m)), with a similar wall structure has its own band gap and electronic property, although the changing trends of the band gaps and strain energies with the increase in their radii are quite similar, as illustrated in Fig. 6. The electronic band gaps of all sorts of tubes are positively proportional to their diameters. However, the band gaps of the small size (n,m) tubes, such as the (3,2), (4,2) and (6,3) tubes, are lower than the bulk material. Thus, the (n,m) tubes have potential and can be prepared for absorbing the visible spectrum of solar energy. In ad-

dition, titanium dioxide nanotubes, with walls containing many unsaturated bridging oxygen atoms and unsaturated titanium atoms, have a good capacity for the absorption of carbon monoxide, hydrogen and methanol, etc.

References

[1] Enyashin A N, Gemming S and Seifert G 2007 *Materials for Tomorrow Springer Series in Materials Science* vol 93 p 33

[2] Shankar K, Mor G K, Prakasam H P, Yoriya S, Paulose M, Varghese O K and Grimes C A 2007 *Nanotechnology* **18** 065707

[3] Mogilevsky G, Chen Q, Kulkarni H, Kleinhammes A, Mullins W M and Wu Y 2008 *J. Phys. Chem.* **112** 3239

[4] Ramirez A F and Morales R Y 2007 *Chem. Mater.* **19** 2947

[5] Chen Q, Zhou W, Du G H and Peng L M 2002 *Adv. Mater.* **14** 1208

[6] Nakahira A, Kato W, Tamai M, Isshiki T, Nishio K and Aritani H 2004 *J. Mater. Sci.* **39** 4239

[7] Wang Y Q, Hu G Q, Duan X F, Sun H L and Xue Q K 2002 *Chem. Phys. Lett.* **365** 427

[8] Akita T, Okumura M, Tanaka K, Ohkuma K, Kohyama M, Koyanagi T, Date M, Tsubota S and Hatuta M 2005 *Surf. Interface Anal.* **37** 265

[9] Kasuga T, Hiramatsu M, Hoson A, Sekino T and Niihara K 1999 *Adv. Mater.* **11** 1307

[10] Ferrari A M, Szieberth D and Noel Y 2011 *J. Mater. Chem.* **21** 4568

[11] Orzali T, Casarin M, Granozzi G, Sambi M and Vittadini A 2006 *Phys. Rev. Lett.* **97** 156101

[12] Vittadini A and Casarin M 2008 *Theor. Chem. Acc.* **120** 551

[13] Enyashin A N and Seifert G 2005 *Phys. Status Solidi* B **242** 7 1361

[14] Ferrari A M, Szieberth D, Claudio M, Wilson Z and Demichelis R 2010 *J. Phys. Chem. Lett.* **1** 2854

[15] Bandura A V and Evarestov R A 2009 *Surf. Sci.* **603** 117

[16] Aradi B and Hourahine B and Frauenheim T 2007 *J. Phys. Chem.* **111** 5678

[17] Yang J, Jin Z, Wang X, Li W, Zhang J, Zhang S, Guo X and Zhang Z 2003 *Dalton Trans.* **20** 3898

[18] Tang H, Berger H, Schmid P E, Levy F, Burri G 1993 *Solid State Commun.* **87** 847

[19] Szieberth D, Ferrari M A, Noel Y and Ferrabone M 2010 *Nanoscale* **2** 81

[20] Wang J G, Wang L, Ma L, Zhao J J, Wang B L and Wang G H 2009 *Physica* E **41** 838

[21] Liu Z J, Zhang Q and Qin L C 2007 *Solid State Commun.* **141** 168

[22] Casarin M, Vittadini A and Selloni A 2009 *ACS Nano* **3** 317